# What are Methylammonium and Solvent Fates upon Halide Perovskite Thin-Film Preparation and Thermal Aging?

Daming Zheng, Fei Chen, Marie-noelle Rager, Liam Gollino, Boxue Zhang, Thierry Pauporté

**Please cite this paper as** : D. Zheng, F. Chen, M.N. Rager, L. Gollino, B. Zhang, Th. Pauporté, What are Methylammonium and Solvent Fates upon Halide Perovskite Thin Film Preparation and Thermal Aging? Adv. Mater. Interfaces, (2022) 2201436. DOI : 10.1002/admi.202201436

# What are Methylammonium and Solvent Fates upon Halide Perovskite Thin Film Preparation and Thermal Aging?

D. Zheng,*[a#] F. Chen,[a#] M.N. Rager,[b] L. Gollino,[a] B. Zhang,[a] and Th. Pauporté*[a]

[a] Institut de Recherche de Chimie Paris (IRCP), UMR8247, Chimie ParisTech, PSL University, CNRS 11 rue P. et M. Curie, F-75005 Paris, France.

[b] NMR Facility, Chimie ParisTech, PSL University, Rue P. et M. Curie, F-75005 Paris, France.

* Authors for correspondence: E-mail: daming.zheng@chimieparistech.psl.eu; thierry.pauporte@chimieparistech.psl.eu

[#] These two authors contributed equally to the work.

**Abstract** :

The recent remarkable achievements in terms of efficiency performance and stability of hybrid organic-inorganic perovskite solar cells (PSCs) have been notably obtained by optimizing the A-site cation composition of formamidinium-based 3D perovskites. As methylammonium chloride is ubiquitously employed in precursor solution for very high efficiency formamidinium-based PSC, the purpose of the present paper is to unveil the exact role of methylammonium ($MA^+$), chloride and solvent on the film growth and their fate upon the layer thermal annealing process. Methylammonium is shown to react with formamidinium to form two methyl compounds while its excess is eliminated along with chloride. The final perovskite layer A-sites are mainly occupied by formamidinium, whereas $MA^+$ content is only 2-3 mol%, and below *3-N*-Methyl formamidinium one. *1-N*-Methyl formamidinium is detected as traces. Meanwhile, the solvent is homogeneously eliminated throughout the layer thickness. Upon thermal aging stress, the layer is degraded from its top with the formation of $PbI_2$. $MA^+$ is rapidly fully eliminated while the stable methyl formamidinium compounds remain in the perovskite layer.

**Keywords** : Halide perovskite layer; Cations reactivity upon thermal annealing; methyl formamidinium; Nuclear Magnetic Resonance NMR; Thermal aging.

**Please cite this paper as** : D. Zheng, F. Chen, M.N. Rager, L. Gollino, B. Zhang, Th. Pauporté, What are Methylammonium and Solvent Fates upon Halide Perovskite Thin Film Preparation and Thermal Aging? Adv. Mater. Interfaces, (2022) 2201436. DOI : 10.1002/admi.202201436

## 1. Introduction

The rapid expansion of researches on perovskite solar cells (PSCs) has been driven by many favorable chemical and opto-electronic properties of hybrid organic/inorganic perovskites compounds such as their low-cost and mild-temperature solution processability, bandgap tunability, high absorption coefficient, low recombination rate, and long diffusion length and high mobility of their charge carriers.[1-7] It has resulted in a rapid rise in the record power conversion efficiency (PCE) of PSCs which lies now beyond 25%.[8-12] These impressive progresses in the efficiency performance have been the results of an in-depth work on the perovskite material itself and on the interfacial engineering with the development of buffer layers of various compositions.[13-23] Compositional engineering plays a key part in achieving highly efficient and stable PSCs and it is noticeable that the works reporting efficiencies above 24% are based on perovskite compounds with a composition mixing both formamidinium ($FA^+$) and methylammonium ($MA^+$) monovalent cations in the A-site of the perovskite structure. The investigated compositions range from $FA_{1-x}MA_xPbI_3$,[13-19] to various compositions mixing more monovalent cations ($MA^+$, $FA^+$, $Cs^+$) along with I and Br halides.[20-23] Amazingly, a careful scrutinizing of the perovskite precursor solution (PPS) composition in these references reveals that MACl is always employed and seems to play a key role in high performance achievement.[13-23]

Formamidinium-rich lead iodide formulations have focused much attention to target a bandgap approaching the Shockley-Queisser optimum.[24] However, due to the large size of $FA^+$, a lattice distortion is induced under ambient conditions, producing a phase transformation into the non-perovskite δ-phase. To overcome this problem and stabilize the black perovskite α-phase, one or more smaller cations, especially $MA^+$, can be added. However, $MA^+$ has undesired properties that jeopardize the long-term stability of the devices. $MA^+$ is a hydrophilic compound and moisture is detrimental for the perovskite stability. It can also form methylamine by deprotonation that outgases with time [25,26] and it degrades under various stressors,[24,26] such as heat, producing iodomethane which is gas released.[27] Moreover, a classical approach to introduce $MA^+$ cation in the perovskite film is to employ an excess of $MA^+$-based precursor in the precursor solution. Upon the preparation process, $MA^+$ will be mostly eliminated while only a small fraction will be integrated into the lattice. In a previous work, we have introduced liquid NMR measurements to accurately quantify the organic cations in perovskite thin films employed in high efficiency solar cells that have been produced from non-stoichiometric precursor solutions.[14] We have found that, when MACl is used as an additive between 20

and 55 mol% of $PbI_2$, most of $MA^+$ is eliminated upon thermal annealing.[14] The remaining amount has been supposed to correspond to the quantity required for the thermodynamical stabilization of the layer. Liquid NMR also allowed us to show the presence in the final layer of products formed by the methylation of formamidinium.

If MACl is ubiquitously employed in very high efficiency PSC, its behavior and exact role on the film growth remain to be unveiled. Moreover, another important question is the fate of $MA^+$ present in the lattice upon aging, especially upon thermal stress. In the present work we have employed a liquid NMR technique to directly follow the fate of methylammonium and soaking solvent upon the thermal annealing process (TAP) utilized for the preparation of films actually used in final photovoltaic devices. The transient and final compositions of the $FAPbI_3$ perovskite film prepared with MACl have been unveiled by this technique. These data have been completed by glow discharge optical emission spectroscopy (GD-OES) measurements which have allowed us to follow the kinetics of $MA^+$ and solvent eliminations and their elimination profile evolution. Moreover, we show that $MA^+$ partly reacts with formamidinium after deprotonation to produce methyl-formamidinium compounds. We give the mechanism of these reactions. We have also investigated the thermal aging of the layers. We reveal that $MA^+$ is further removed then and that the lattice shrinks. After a few hours, $MA^+$ is almost fully eliminated while the stable methyl-formamidinium products remain in the layer.

## 2. Results and discussion

### *2.1. Effect of MACl additive on the perovskite layer formation.*

As a key compound for reaching high efficiency, the exact role and fate of MACl on the perovskite film formation remain to be fully understood. We focused our attention on the preparation of $FAPbI_3$ perovskite films. We employed the precursor solution optimized in our previous works,[14,15] in which FAI, $PbI_2$ and MACl at 48 mol% of $PbI_2$ are mixed. The details about the solar cells properties and performances can be found in Refs[14] and [15]. The prepared PSCs reached a maximum power conversion efficiency of 22.2% after the addition of a capping layer formed by treating the perovskite film surface by a 2-phenylethylammonium iodide (PEAI) solution (**Table S1**, Supporting Information). The $FAPbI_3$ PSC, prepared without MACl additive, reached a PCE of only 14.3 % measured on the reverse scan and exhibited a large hysteresis (Control sample) (**Table S1,** Supporting Information).

**Please cite this paper as** : D. Zheng, F. Chen, M.N. Rager, L. Gollino, B. Zhang, Th. Pauporté, What are Methylammonium and Solvent Fates upon Halide Perovskite Thin Film Preparation and Thermal Aging? Adv. Mater. Interfaces, (2022) 2201436. DOI : 10.1002/admi.202201436

Precursor thin films were first prepared by spin-coating and chlorobenzene anti-solvent dripping. As discussed below in more details, without MACl, their XRD pattern exhibited a δ-phase diffraction peaks at 11.80°, while, with MACl, the perovskite α-phase was detected at 13.97° along with a small amount of δ-phase. The films were then thermally annealed at 153°C to complete the crystallization. The maximum PCE was attained for 13 min of thermal annealing time. The layer components evolution upon TAP were followed from their proton nuclear magnetic resonance ($^1$H NMR) spectra. For each annealing time, several films were dissolved in deuterium dimethyl sulfoxide (DMSO-d6) and the resulting solutions were analyzed by liquid $^1$H-NMR as shown in **Figure 1a**.

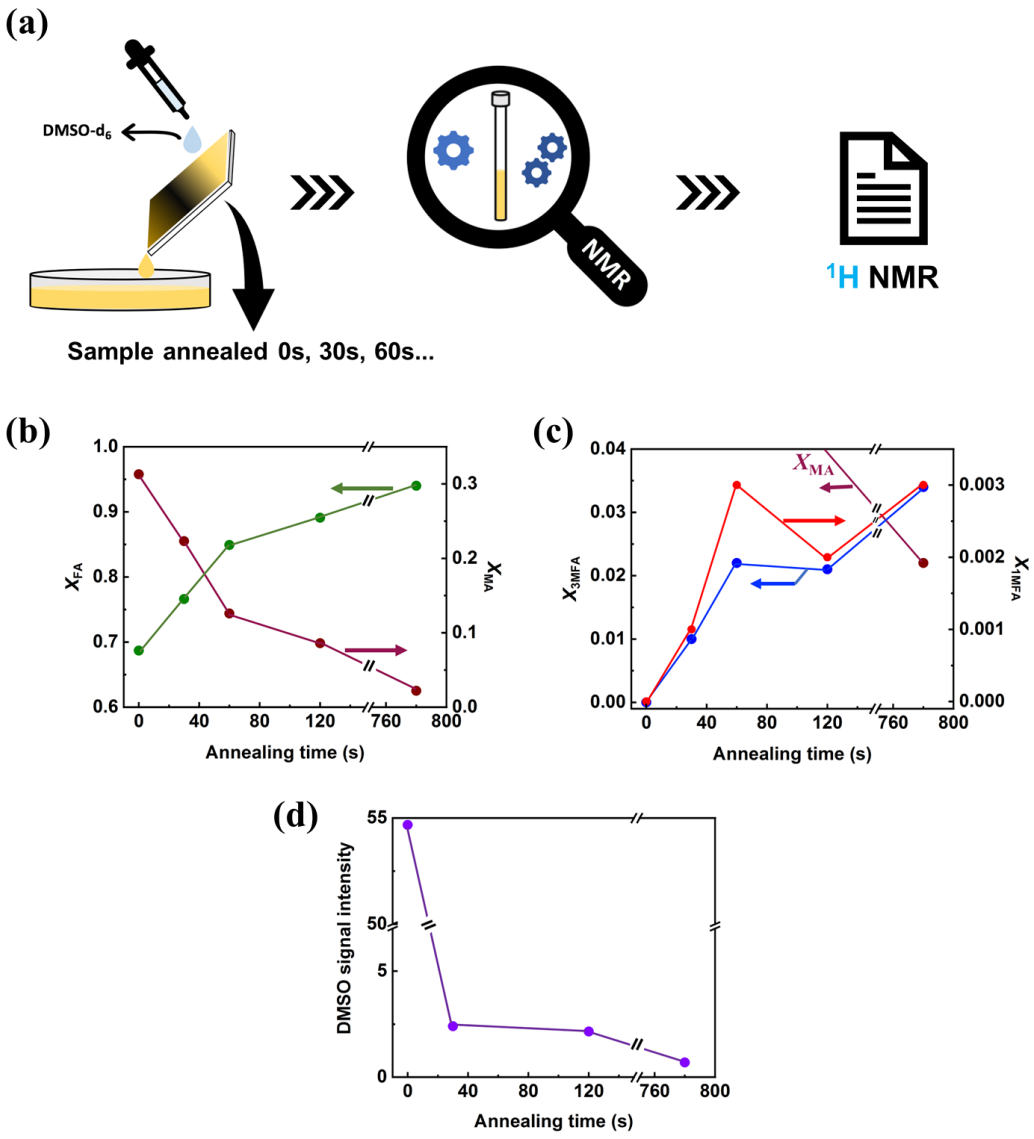


**Figure 1**. (a) Preparation process of NMR perovskite films samples. (b) $x_{FA}$ and $x_{MA}$ layer values measured by $^1$H-NMR for various thermal annealing times. (c) Variation of $x_{3MFA}$ and $x_{1MFA}$, measured

by NMR, with the thermal annealing time. (d) Variation of the $^{1}$H-NMR protonated DMSO signal intensity (singlet at δ=2.54 ppm) with the layer annealing time.

The liquid-state $^{1}$H-NMR spectra for increasing annealing times are reported in **Figures S1a-e** (Supporting Information). For the initial precursor layer (**Figure S1a**), $^{1}$H signals were found at δ = 2.37 ppm and δ = 7.84 ppm which agree with the methyl (C***H*₃**) signal in $MA^+$ and the methyne (C***H***) signal in $FA^+$, respectively (reference spectra in **Figure S1f** and **S1g**, Supporting Information, also confirmed by $^{13}$C-NMR). The spectrum also exhibited solvent with the peak at δ = 2.54 ppm assigned to the $^{1}$H methyl signal of the soaking dimethylsulfoxide (DMSO) present in the initial layer. Signals at δ = 2.73 ppm, 2.89 ppm and 7.95 ppm are attributed to dimethyl formamide (DMF) solvent. After 30 s of layer thermal annealing, (**Figure S1b**, Supporting Information) the intensity of the $MA^+$ peak at δ = 2.37 ppm was decreased due to the elimination of this compound. We also observed a strong decrease of the DMSO peak at δ = 2.54 ppm. A third interesting feature is that two new proton signals appeared at δ = 2.81 ppm and δ = 2.96 ppm. They could be indexed owing to reference products prepared by reacting methylamine and formamidinium iodide [25] and measured by NMR (**Figure S1h,** Supporting Information). They allowed us to assign δ = 2.81 ppm to the methyl (C***H*₃**) signal of *3-N*-Methylformamidinium (C***H*₃**-$NH_2$-CH=$NH_2^+$), noted $3MFA^+$, and the second signal (δ = 2.96 ppm) to *1-N*-Methyl formamidinium ($NH_3^+$-CH=N-C***H*₃**), noted $1MFA^+$. The reference spectrum of *1N-3N*-dimethylformamidinium ($CH_3$-$NH_2^+$-CH=N-$CH_3$, noted DMFA) (**Figure S1i,** Supporting Information) is characterized by two $^{1}$H signal at 2.79 ppm and 3.02 ppm. The first one is assigned to the methyl group of C***H*₃**-NH-, while the second is assigned to the other methyl group, C***H*₃**-N=. This compound was not clearly detected in the layers, even after the full thermal annealing process. $3MFA^+$ and $1MFA^+$ can be formed by the reaction of methylamine, the $MA^+$ deprotonation product (**Scheme 1A**), with $FA^+$ through addition-elimination reactions. **Scheme 1B** summarizes the reactions that occur in the layers according to our NMR results. In **Scheme 1C**, we also consider the possible formation of DMFA produced by reacting MA with $3MFA^+$ or $1MFA^+$.

For 1 min (**Figure S1c**), 2 min (**Figure S1d**) and 13 min (**Figure S1e**) annealing times, the trend was the decrease of the $MA^+$ and DMSO signals while those of $3MFA^+$ and, in a less extent, $1MFA^+$ increased. The first important conclusions are that (i) the final layer is a mixed organic cation perovskite which contains $FA^+$, $MA^+$, $3MFA^+$ and $1MFA^+$ and that (ii) the two

latter cations are formed by addition-elimination upon the layer TAP at 153 °C. We also noted that $DMFA^+$ was not clearly detected (only traces in some samples).

**Table 1**. Molar fractions of organic A-site cations in the layers. Initial composition and for increasing annealing at 153 °C times.

| Annealing time | $x_{FA}$ | $x_{MA}$ | $x_{3MFA}$ | $x_{1MFA}$ |
|---|---|---|---|---|
| 0s | 0.687 | 0.313 | 0 | 0 |
| 30s | 0.766 | 0.223 | 0.010 | 0.001 |
| 60s | 0.849 | 0.126 | 0.022 | 0.003 |
| 2 min | 0.891 | 0.086 | 0.021 | 0.002 |
| 13 min | 0.940 | 0.022 | 0.034 | 0.003 |

The signal peaks have been integrated and reported to one H for each organic cation. We have then quantified the global molar fraction for each of them ($x_{FA}$, $x_{FA}$, $x_{1MFA}$, $x_{3MFA}$) at increasing thermal annealing time periods as described in the **Section B** (Supporting Information). The residual hydrogen signal of deuterated DMSO peak (quintuplet at $\delta$ = 2.50 ppm) was used as an internal reference. The results are gathered in **Table 1**. In the initial layer, $x_{MA}$ was measured at 0.313 by NMR. This value is very close to the stoichiometry in the precursor solution (0.325) and therefore it validates our approach to titrate the cations in the layer by liquid NMR. The absence of $3MFA^+$, $1MFA^+$ and $DMFA^+$ in the initial layer (0s) reveals that these cations were not generated in the precursor solution used in this study and that the addition-elimination reactions did not occur upon the PPS preparation and storage, as well as upon the spin-coating and dripping steps. **Figure 1b** shows that $x_{MA}$ continuously decreased upon the TAP due to the volatilization of methylammonium after deprotonation. At the end of this annealing step, after 13 min, $x_{MA}$ was found at the very low level of 0.02-0.03. This is in good agreement with our previous report.[14] Another important finding is that the condensation products appeared upon the thermal annealing at 153 °C and that their quantity increased with the annealing time. The predominant product was $3MFA^+$ while $1MFA^+$ was formed in a 10 times less extent. These two compounds have been produced by proton transfer from methylamine (**Scheme 1B**). We have performed thermodynamical calculations which agree with our titration results (**Figure S2a**, Supporting Information). They show that the reaction between FAI and MA is spontaneous, and that $3MFA^+$ is more stable than $1MFA^+$. We

**Please cite this paper as** : D. Zheng, F. Chen, M.N. Rager, L. Gollino, B. Zhang, Th. Pauporté, What are Methylammonium and Solvent Fates upon Halide Perovskite Thin Film Preparation and Thermal Aging? Adv. Mater. Interfaces, (2022) 2201436. DOI : 10.1002/admi.202201436

have also considered the further reactions of $1MFA^+$ and $3MFA^+$ with methylamine as shown in **Scheme 1C**. This reaction is more difficult (**Figure S2b**, Supporting Information), and it explains the absence of clearly detectable $DMFA^+$ in the perovskite layers, even after the TAP completion. Finally, it is noticeable that the final $3MFA^+$ content was slightly higher than the $MA^+$ one (**Table 1**). The deprotonation of $MA^+$ is a thermally activated reaction.

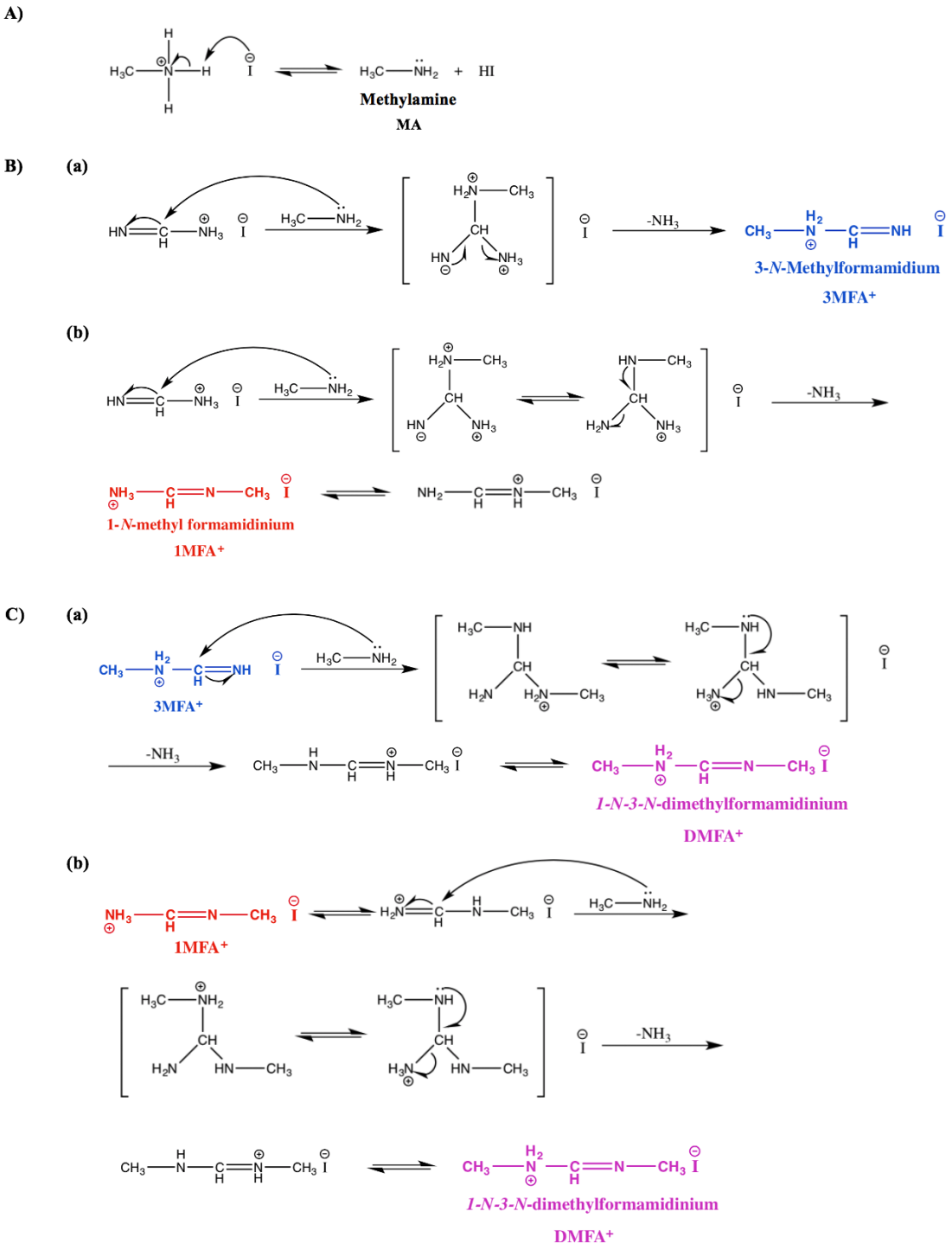


**Scheme 1**. Possible reaction mechanisms of methyl-formamidinium compounds formation by addition-elimination.

As the organic cation size is an important parameter for the perovskite structure stabilization, we have drawn the five organic cations molecular structures and calculated their maximum length in **Figure S3** (Supporting Information). The stability of the perovskite compounds has been reported to depend on their Goldschmidt tolerance factor, $t_G$ [28,29] defined as :

$$t_G = \frac{r_A + r_B}{\sqrt{2}(r_B + r_X)} \qquad (1)$$

where $r_A$, $r_B$ and $r_X$ are the ionic radii of A, B and X ions, respectively, in $ABX_3$ and are reported in **Table S2** (Supporting Information). For pure $FAPbI_3$, $t_G$ is 0.987. This value is slightly higher than the ideal one and $FAPbI_3$ is supposed to easily lead to the formation of the yellow δ-phase. $t_G$ of the methyl formamidinium compounds are higher due to the bigger size ($r_A$) of $MFA^+$. It is calculated at 1.041 for $(3MFA)PbI_3$. Since the large cations cannot enter into the 3D perovskite lattice, we conclude that they must be located at defects and/or at grain boundaries. Interestingly, the shape and size of the methyl formamidinium monocations involved here are similar to those of hydroxyethylammonium ($HEA^+$) and thioethylammonium ($TEA^+$) which have been shown to substitute $PbI^+$ units in lead-deficient perovskites and to stabilize the 3D perovskite structure in Ref.[10,28,30] A similar phenomenon could then be involved in the present case where $3MFA^+$ and $1MFA^+$ would substitute lead and iodide charged vacancies.

Based on the above discussion, we have also analyzed the effect of MACl additive amount in PPS on the organic cation composition of the final $FAPbI_3$/MACl layers. MACl in the precursor solution was varied between 20 mol% to 55 mol% of $PbI_2$. All the layers were annealed for 13 min. **Table 2** shows the molar fraction of the four organic cations calculated from NMR data reported in **Figure S4** (Supporting Information). Up to 40 mol% of MACl, we found that $MA^+$ and methyl formamidinium cations increased continuously and that $MA^+$ content was close to the $3MFA^+$ one. Above, the composition was constant within the uncertainty of the titration method. We can then suppose that the system has reached a composition optimum in terms of entropic stabilization. In our previous work [14], we have shown that the PCE continuously increases from 20 mol% to 48 mol% and then decreases (see also **Table S1**, Supporting Information). The 48 mol% samples exhibited the best structural and morphological quality and a monolithic structure.

**Please cite this paper as** : D. Zheng, F. Chen, M.N. Rager, L. Gollino, B. Zhang, Th. Pauporté, What are Methylammonium and Solvent Fates upon Halide Perovskite Thin Film Preparation and Thermal Aging? Adv. Mater. Interfaces, (2022) 2201436. DOI : 10.1002/admi.202201436

**Table 2**. Fraction of the organic A-site cations in the final perovskite layer as a function of the MACl mol% added in the precursor solution.

| MACl/ | $x_{FA}$ | $x_{MA}$ | $x_{3MFA}$ | $x_{1MFA}$ |
|---|---|---|---|---|
| 20 mol% | 0.966 | 0.014 | 0.018 | 0.002 |
| 30 mol% | 0.953 | 0.022 | 0.022 | 0.003 |
| 40 mol% | 0.934 | 0.030 | 0.032 | 0.004 |
| 48 mol% | 0.934 | 0.024 | 0.038 | 0.004 |
| 55 mol% | 0.937 | 0.026 | 0.033 | 0.004 |

NMR measurements also revealed that the initial precursor film contained soaking solvents. Protonated DMSO was detected at δ = 2.54 ppm in a rather large quantity because DMSO interacts with Pb-I precursors and cannot be fully eliminated by the antisolvent dripping.[31] DMF was also detected, but as a trace (signals at δ = 2.73 ppm, 2.89 ppm and 7.95 ppm). The variation of the DMSO content with the TAP time in **Figure 1d** reveals that this solvent is rapidly eliminated from the layer and that a low level is found after only 30s.

**Please cite this paper as** : D. Zheng, F. Chen, M.N. Rager, L. Gollino, B. Zhang, Th. Pauporté, What are Methylammonium and Solvent Fates upon Halide Perovskite Thin Film Preparation and Thermal Aging? Adv. Mater. Interfaces, (2022) 2201436. DOI : 10.1002/admi.202201436

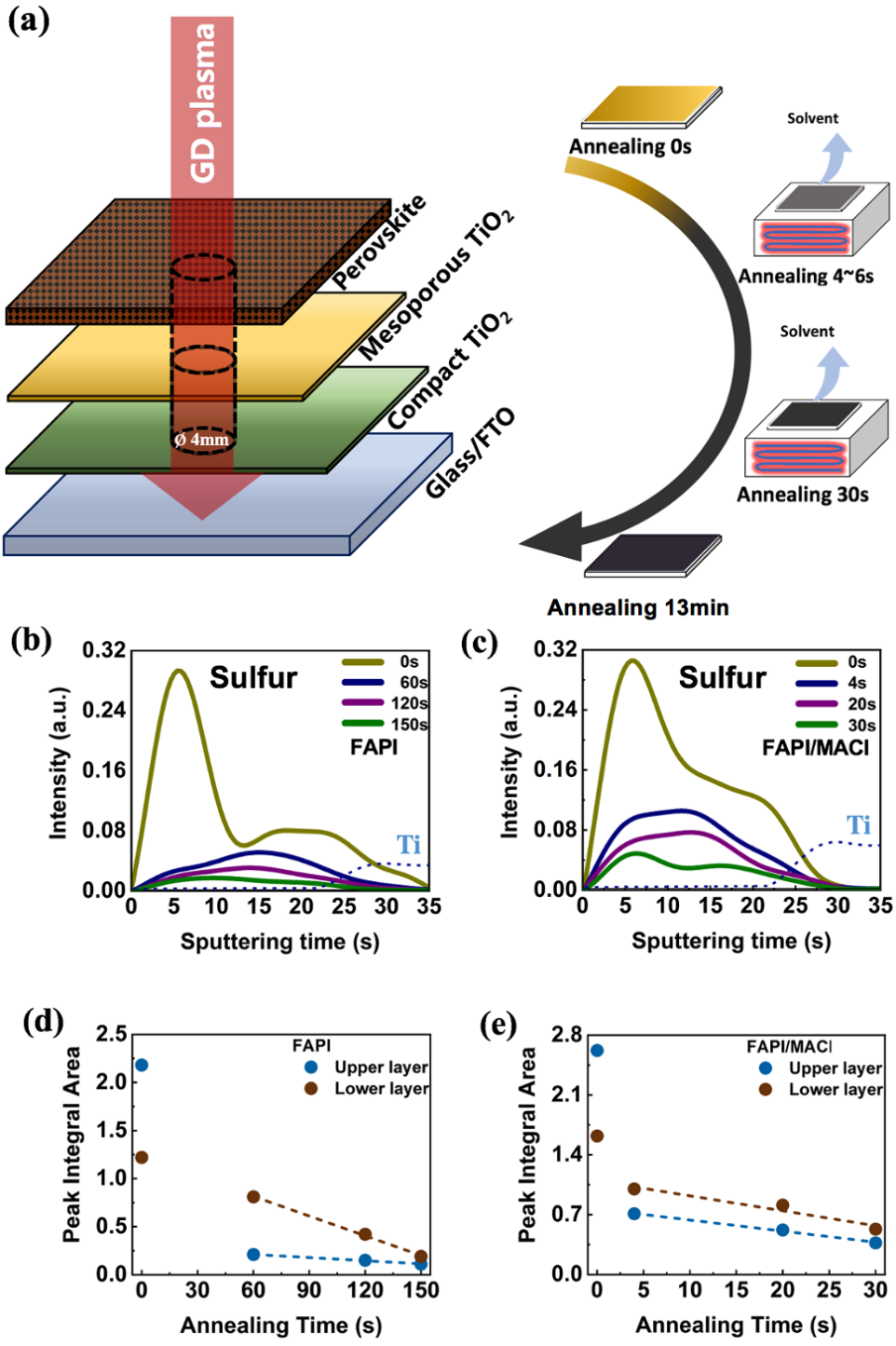


**Figure 2**. (a) Left: Investigated solar cells architecture with the scale of the GD plasma beam which abrades gradually the structure with time. The detection diameter is 4 mm. Right: film annealing process. (b,c) Evolution of GD-OES sulfur element (S) profile in the (b) FAPI and (c) FAPI/MACl layers upon thermal annealing. (d,e) Peak integral area of upper layer and lower layer at increasing annealing time. (Blue dashed line: linear fit line of upper layer. Brown dashed line: linear fit line of lower layer).

The GD-OES technique was employed to further uncover the DMSO solvent elimination mechanism. In this technique, an argon plasma is created which progressively ablates the sample surface in a plane-parallel manner (**Figure 2a**). The released sample atoms, are excited prior to emit light upon their deexcitation. The analysis of the emitted spectrum gives the sample elemental composition in real time. Since sulfur is only present in DMSO, we followed the variation of sulfur profiles with the TAP time (**Figure 2a-c** and **Figure S5a,b** Supporting Information). The FAPI/MACl curves are disclosed in **Figure 2c**. We observed that the solvent was mostly localized in the upper part of the layer (short sputtering time). During the first annealing seconds, the soaking solvent was rapidly eliminated, especially the fraction localized near the surface. After 4 s, we observed that DMSO was rather homogeneously eliminated throughout the layer by volatilization. We compared the behavior of our system with a control sample, free of MACl additive ($FAPbI_3$) in **Figure 2b**. We found again a large amount of solvent in the top part of the layer. It was quickly eliminated while the inner solvent was more difficult to remove. To visualize the kinetic of solvent elimination, we divided the layer into an inner and an upper part, as described in our previous work [32] and in the Supporting Information (**Figure S6** and related comment, Supporting Information). We then quantified the solvent content in these layers by integrating the curves. **Figure 2d and 2e** report the integration values at increasing TAP time without and with MACl additive, respectively. The fast elimination of the solvent during the first seconds is confirmed in both cases. For $FAPbI_3$, the slope is much higher for the inner (lower) layer compared with the outer (upper) layer. It is the signature of an upward growth (from bottom to top). On the other hand, the two slopes are close for the FAPI/MACl system. It shows that the solvent is homogeneously eliminated in this case. It results in large perovskite grains and in a monolithic structure as shown in **Figure S7** (Supporting Information).

GD-OES technique was also employed to further investigate the fate of MACl in the layer upon TAP. **Figure 3a** shows the evolution of the carbon element profile and **Figure 3b** figures out the integration over the full profile. The initial curve is characterized by a C-peak in the upper layer part (short sputtering time). It fits with the S curve in **Figure 2c** and is assigned to the soaking solvent. This peak disappears during the first 4s of TAP. This result agrees with the NMR study. Then, for longer annealing time, a small decrease of the peak integral area is found (**Figure 3b**). Based on our NMR result, it corresponds to the elimination of $MA^+$ which is slower than the solvent elimination. We have also followed the chlorine profile evolution upon the layer TAP in **Figure 3c**. Chlorine originates from MACl. The integral of the profile is

**Please cite this paper as** : D. Zheng, F. Chen, M.N. Rager, L. Gollino, B. Zhang, Th. Pauporté, What are Methylammonium and Solvent Fates upon Halide Perovskite Thin Film Preparation and Thermal Aging? Adv. Mater. Interfaces, (2022) 2201436. DOI : 10.1002/admi.202201436

reported at various annealing times in **Figure 3d**. It is observed that Cl is continuously eliminated from the layer. Most of Cl is eliminated during the first 2 min of TAP. The curve follows the carbon one because chloride is eliminated with methylammonium. Only traces of Cl are present in the final layer.

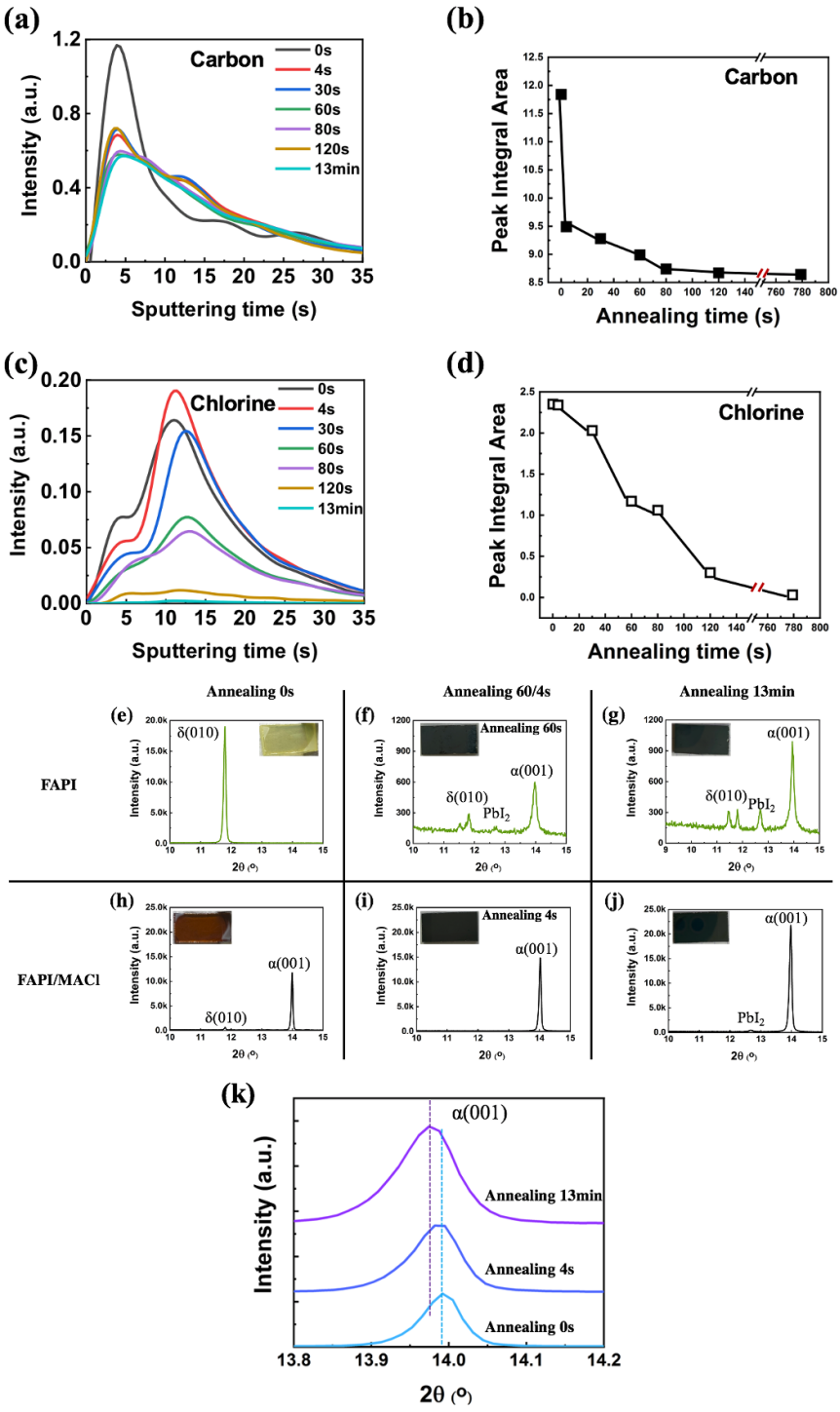


**Figure 3**. (a) Evolution of GD-OES carbon element profile in the FAPI/MACl layer upon thermal annealing and (b) corresponding peak integral area. (c) Evolution of GD-OES chlorine element profile in the FAPI/MACl layer upon thermal annealing and (d) corresponding peak integral area upon thermal

annealing. (e-g) XRD patterns of FAPI films upon thermal annealing. (i-j) XRD patterns of FAPI/MACl films upon thermal annealing and (k) zoom view of the α(001) diffraction peak.

We also measured the XRD patterns of the layers upon the TAP of samples without and with MACl additive. In the control layer, the initial crystallized fraction of $FAPbI_3$ was pure non-perovskite δ-phase (δ(010) at 11.80°) and the samples were yellow colored (**Figure 3e**). On the other hand, the sample with MACl was brown, contained mainly the α-phase (α(001) at 13.97°) with a small fraction of δ-phase. The benefits of MACl additive includes the stabilization of the α-phase (**Figure 3h**).[13,14] The control layer, after 60s of annealing time, presented a rather broad α-phase peak, $PbI_2$ at 12.7° and the δ-phase at 11.80°. After completion of the TAP, these three phases were already present and the crystallinity was better. A close look at **Figure 3f** and **Figure 3g** for short and long FAPI annealing times shows a peak splitting with a second peak at 11.45° and 11.55°, respectively. Such spitting has been observed upon aging under a humid environment [33] but its origin in the present case remains to be clarified. For the MACl containing sample, the α-phase peak intensity continuously increased and the final crystallinity was high. **Figure 3k** compares the α(001) perovskite peak position. A left-shift was found with TAP which corresponds to a lattice parameter enlargement. Based on the NMR results, it is assigned to the MA elimination and to the formation of the methyl compounds. The easier crystallization of the perovskite in the presence of MACl was confirmed by differential scanning calorimetry (DSC).[34] In **Figure S8a** (Supporting Information) the α-phase crystallization process, defined by the third endothermic peak in our previous work [35], ends at 153.5°C in the absence of additive. Adding MACl reduces this temperature to 123.5°C (**Figure S8b** Supporting Information) and it is concluded that this additive renders the crystallization easier.

*2.2. Thermal aging of the layers.*

The previous section has highlighted the complex behaviour of MACl upon the film formation process, especially during the thermal annealing. A striking result is that, in the final film, only a small amount of $MA^+$, at about 2-3% molar fraction of A-site cation, remains in the layer to stabilize the structure. As solar panels undergo various stress, notably thermal stress, an important question is then what happens to the layer when it is submitted to rather high temperatures. To get insights into the behavior of organic A-site cations upon thermal aging,

we conducted NMR, GD-OES, XRD and optical measurement investigations to follow the changes occurring in the perovskite film upon heating in a $N_2$ atmosphere at 130°C.

The NMR spectra are disclosed in **Figure S9a-d** (Supporting Information). We have followed the change in the global molar fraction for each A-site organic cation ($x_{FA}$, $x_{MA}$, $x_{3MFA}$, $x_{1MFA}$) with the thermal aging (**Table 3**). It is remarkable that $MA^+$ is rapidly eliminated during the first heating hours, while $x_{3MFA}$ slightly increases and $x_{1MFA}$ remains low. Between 10h and 20h aging time, no compositional change was found. As newly considered cations in perovskite layer, we measured the thermal stability of N-Methyl formamidinium by differential scanning calorimetry. We found that the 3MFAI and 1MFAI mixture was stable up to 200 °C (see **Figure S8c,d**, Supporting Information).

**Table 3**. Molar fraction of the organic A-site cations in the initial layer and for increasing thermal stress aging times at 130°C in $N_2$.

| Aging time | $x_{FA}$ | $x_{MA}$ | $x_{3MFA}$ | $x_{1MFA}$ |
|---|---|---|---|---|
| 0 h | 0.940 | 0.022 | 0.034 | 0.003 |
| 4h | 0.948 | 0.007 | 0.041 | 0.004 |
| 10 h | 0.952 | 0.003 | 0.042 | 0.003 |
| 20 h | 0.951 | 0.004 | 0.042 | 0.003 |

**Please cite this paper as** : D. Zheng, F. Chen, M.N. Rager, L. Gollino, B. Zhang, Th. Pauporté, What are Methylammonium and Solvent Fates upon Halide Perovskite Thin Film Preparation and Thermal Aging? Adv. Mater. Interfaces, (2022) 2201436. DOI : 10.1002/admi.202201436

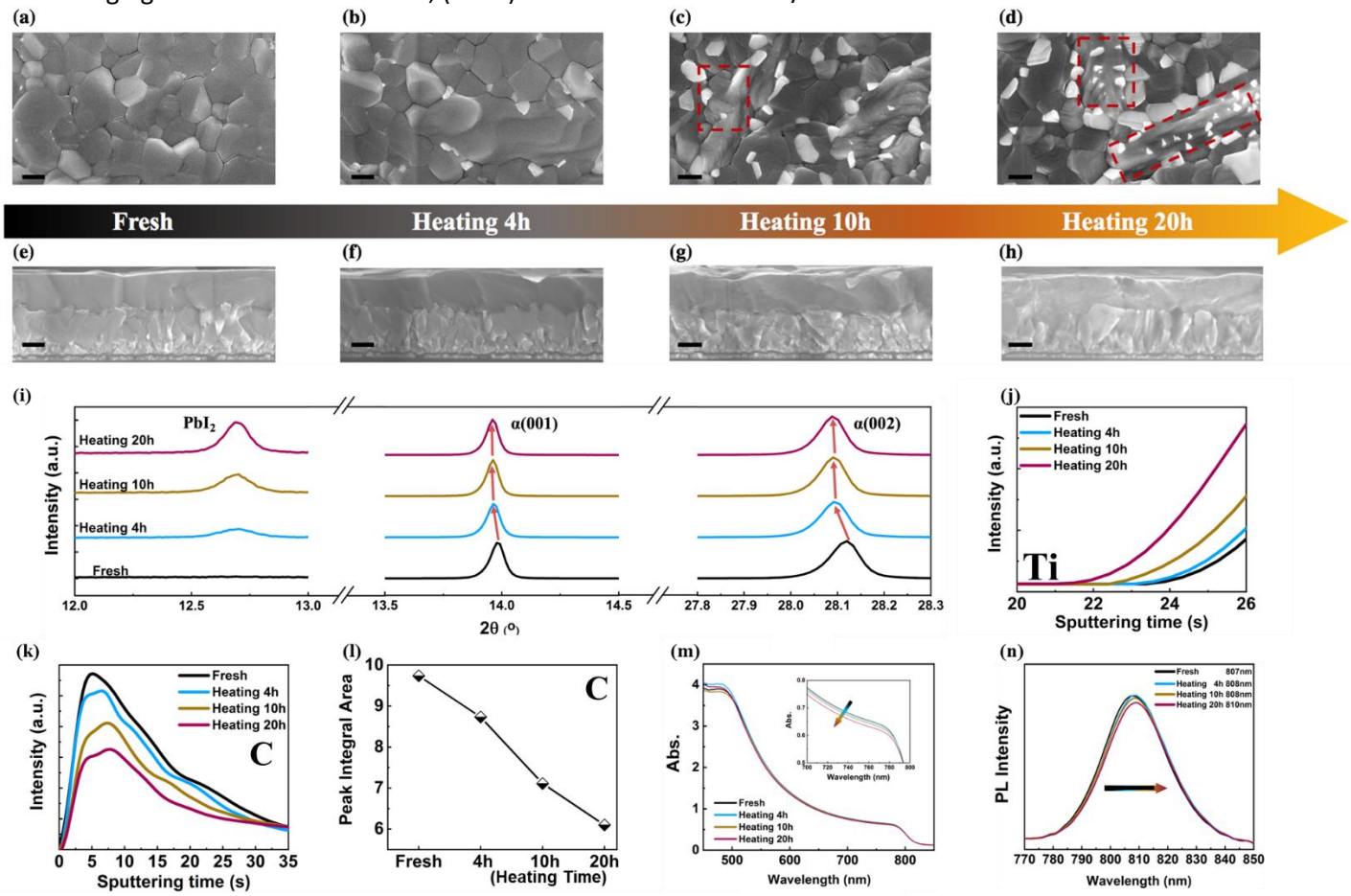


**Figure 4**. Effects of perovskite aging at 130°C in $N_2$ atmosphere on (a-d) SEM top view (scale bar 1 µm) and (e-h) cross-sectional view (scale bar 300 nm). The red boxes outline the $PbI_2$ grain formation. (i) On the XRD pattern of the perovskite layer. (j) GD-OES profile curve of titanium (Ti) and (k) carbon (C) elements. (l) Integrals of Carbon GD-OES profile curves. (m) Absorbance and (n) photoluminescence (PL) spectra.

The XRD patterns in **Figure 4i** and **Figure S10** (Supporting Information) show the appearance of $PbI_2$ after 4h of thermal aging time and an increase of the $PbI_2$ content with time. $PbI_2$ is the perovskite degradation product. The analysis of the α(001) and α(002) peak positions (**Figure 4i**) shows a left shift with time. It is the result of the lattice expansion due to its relaxation and to MA loss. On SEM top views (**Figure 4a-d**) the thermal aging is accompanied by the formation of bright $PbI_2$ grains on the surface. The red boxes outline the formation of multiple small $PbI_2$ grains on large perovskite grains. Their density and size increase with the aging time. $PbI_2$ is the decomposition product of the perovskite material by MA and FA loss. **Figure 4e-h** shows the cross-sectional views of the layers. The initial layer is frankly broken with a monolithic structure and vertical grain boundaries. While the aging time increases, the grains and their boundaries become less and less defined. We have measured the average

thickness of the layers and found 452 ±22 nm, 433 ±21 nm, 427 ±24 nm and 418 ±22 nm for 0 h, 4 h, 10 h and 20 h of aging, respectively. Therefore, the layer degradation results in a progressive decrease of the thickness. The reduction of layer thickness was confirmed by the GD-OES measurements. **Figure 4j** shows the sputtering time at which Ti of the meso-$TiO_2$ layer appears. It shifts progressively to shorter time due to the perovskite layer tapering. **Figure 4k** displays the change in the carbon profile measured by GD-OES with the thermal aging stress. Carbon is preferentially eliminated from the top of the layer. **Figure 4l** is the change of the integral carbon GD-OES curve with time. It continuously decreases in agreement with our previous observations: FAI is gradually eliminated by degradation/volatilization from the top of the layer, the perovskite is degraded in $PbI_2$. This compound forms the bright grains on the surface.

The thermal aging is also accompanied by a slight continuous decrease of the absorbance in the visible/near infrared region (**Figure 4m**). The Photoluminescence spectrum is characterized by a band-to-band peak emission (**Figure 4n**). Its maximum slightly red-shifted with the thermal aging. The analysis of the absorbance band-edge (**Figure S11**, Supporting Information) shows a direct transition and a small shift of the optical bandgap from 1.529 eV for a fresh perovskite layer to 1.525 eV for a 20 h aged one. The slight bandgap reduction and PL shift are assigned to the bulk loss of $MA^+$ and agrees with the lattice expansion.

An interesting question is how the insertion of methyl-formamidinium compounds in the perovskite affects the performance of the solar cells. The above study has shown that a method to prepare FA/3MFA mixed cation perovskite layer is to thermal age FA/MA layers. After 4h at 130°C, the $FAPbI_3$ perovskite contains 4% of $3MFA^+$ and traces of $MA^+$ and $1MFA^+$ (**Table 3**). We have prepared films treated for various times at 130°C (0h, 1h and 4h). The structures were then completed by depositing the SpiroOMeTAD layer and the gold back-contact. The measured *J-V* curves of the devices are presented in **Table S3** (Supporting Information). They show a decrease of the PCE and a slight increase in the HI with the annealing time. We have then compared these cells with $FAPbI_3$ ones, prepared without MACl additive. Their PCEs were higher and they had a significantly lower HI. The difference between the 4h cell and the $FAPbI_3$ one is the presence of 4% of $3MFA^+$ in the former. It shows that $3MFA^+$ has a beneficial effect but less than $MA^+$. It notably helps the blocking of iodide migration and depletes the hysteresis.

## 3. Conclusions

We have highlighted the behavior of MACl and solvent upon the formamidinium lead iodide film formation process. Most methylammonium is eliminated by thermal volatilization along with chloride upon the layer thermal annealing. A small fraction reacts with formamidinium after deprotonation to form mainly *3-N*-Methyl formamidinium, and, in a less extent, *1-N*-Methyl formamidinium. The chemical mechanism of these reactions has been provided. These compounds have not been found in the initial layer, and they are therefore not formed upon the perovskite precursor solution preparation, upon the solution spin-coating and upon the dripping processes. By quantification, we have measured that methylammonium represent only 2-3 mol% of A-site cation in the final perovskite layer, while the *3-N*-Methyl formamidinium content is slightly higher. Due to methylammonium elimination, the lattice parameter slightly increases upon the TAP. We have also shown that MACl favors the crystallization of the α-phase and the homogeneous elimination of the solvent throughout the layer thickness. It results in large grains and in a monolithic structure. Upon thermal aging stress, the layer is degraded from its top with the formation of crystallized $PbI_2$. $MA^+$ is rapidly, almost fully, eliminated while the methyl formamidinium compounds are found thermally stable and remain in the perovskite layer.

## 4. Experimental

Formamidinium iodide and methylammonium chloride were employed as received from Greatcell Solar Materials Pty Ltd and Alfa Aesar, respectively. *N*-Methyl formamidinium and *1N-3N*-dimethyl-formamidinium reference powders were prepared as described in Ref.[24] (See the A.Complementary Experimental section in the Supporting Information). The fluorine-doped $SnO_2$ (FTO) substrates were cleaned and the compact $TiO_2$ hole blocking layer (*c*-$TiO_2$) and the mesoporous $TiO_2$ (*mp*-TiO2) layer were deposited as described in our Ref.[36]. We prepared a mixed cation precursor solution with a 1.2M concentration by mixing 206 mg of formamidinium iodide (FAI, Greatcell Solar Materials Pty Ltd ), 553 mg of $PbI_2$ (TCI), and 38.9 mg of methylammonium chloride (Alfa Aesar) in 800 µL DMF and 200 µL DMSO. The solution was spin-coated on top of the FTO/*c*-$TiO_2$/*mp*-$TiO_2$ substrates. 100 µL of chlorobenzene was dropped upon spinning to produce layers. For the $FAPbI_3$ control films, a precursor solution with a 1.2 M concentration was prepared by mixing 103.2 mg of FAI and 276.7 mg of $PbI_2$ in 100 µL DMSO and 400 µL DMF. The spin coating procedure was the same.

All the layers were annealed at 153°C on a hotplate in a $N_2$ filled glovebox. The final optimized films were annealed for 13 min for the FAPI/MACl films and for 18 min for the $FAPbI_3$ control films. For the aging experiments, the perovskite layers were heated on a hotplate at 130°C in a $N_2$-filled glovebox for a duration of 0 h, 4 h, 10 h and 20h.

The precursor layers were deposited on a sprayed *c*-$TiO_2$ layer and annealed for various times. They were dissolved in DMSO-$d_6$ solvent (99.96 %D, $H_2O$<0.01%, Euriso-top). NMR spectra were recorded on a Bruker Neo 500 spectrometer, using DMSO-d6 as solvent. Chemical shifts are reported in ppm downfield from tetramethylsilane and are referenced to the residual hydrogen signal of deuterated solvent (2.50 ppm) for $^1$H NMR, and the residual solvent carbon signal (39.5 ppm) for $^{13}$C NMR. $^1$H spectra were acquired with a 90° pulse of 10.0 ms, 64K data points over a 10kHz spectral width, an acquisition time of 3.28 s, a recycle delay of 10 s and 256 scans. The Fourier transform was applied to the FID without prior exponential line-broadening. For each spectrum, the integrations were normalized to the residual DMSO-d6 proton signal used as an internal reference (arbitrarily noted 100), allowing comparison of the integrations of the different spectra.

Glow-Discharge Optical Emission Spectroscopy (GD-OES) analyses were performed using a HORIBA Jobin Yvon GD Profiler 2 with Quantum Software. The instrument configuration included a RF-generator (at 13.56 MHz), a standard HORIBA Jobin Yvon glow discharge source with a cylindrical anode of 4 mm internal diameter and two optical spectrometers (a polychromator and a monochromator) for fast-optical detection. No loss in time resolution was ensured thanks to the detection system, composed of independent photomultiplicators (PM), which guarantee simultaneous detection of the signals corresponding to multiple wavelength with spectral resolution of 12 pm. The emission signals of 47 elements were recorded but only the signals of the species of interest are discussed in the paper. The selected wavelength for S, C and Cl were 180.7 nm, 165.7 nm and 135 nm, respectively.

The structure of the organo-lead perovskite films was characterized by a PANanalytical X-Pert high-resolution X-ray diffractometer (XRD) operated at 40 kV and 45 mA and using the CuKα radiation with λ= 1.5406 Å.[37] The morphology of perovskite thin films was imaged using a field-emission SEM equipment (Zeiss Supra 40) in the in-lens mode.

The glass/FTO/c-$TiO_2$/meso-$TiO_2$/perovskite/SpiroOMeTAD/Au solar cells were prepared as described in our Ref.[14,15] The *J-V* curves were recorded by a Keithley 2410 digital

sourcemeter, using a 0.1 $V.s^{-1}$ voltage scan rate. The solar cells were illuminated with a solar simulator (Abet Technology Sun 2000) filtered to mimic AM 1.5G conditions (100 $mW/cm^2$).

*Statistical Analysis*: For NMR, a minimum of 8 films were prepared from the same batch for each condition. They were dissolved in 0.75 mL of deuterated solvent (DMSO-d6). The integration bounds on either side of each NMR peak were the same from one spectrum to another with a margin of error of +/- 5 Hz. Integrations are given with an accuracy of +/- 1% for peaks with a signal-to-noise ratio greater than 10 and 5% for peaks with a S/N greater than 1. GD-OES data come from two different batches for each experimental condition, and the test results obtained were reproducible to ensure the reliability of the obtained data. Because of the repeatability of the data, we selected one batch of data for plotting and integration. For SEM cross-section determination, two samples were prepared and observed for each condition. Six measurements were done on each sample. Data points are represented as mean ± standard deviation.

**Acknowlegements**

We acknowledge Dr. P. Volovitch for the access to the GD-OES equipment and for discussion. The Ph.D scholarship of Fei Zheng and Daming Zheng were funded by the CSC-Paristech program (grant numbers 201904910420 and 201806310126). The ANR agency is acknowledged for financial support via the Moreless project ANR-18-CE05-0026 and the ChemSta project ANR-21-CE05-0022. PSL and Ile de France Region is gratefully acknowledged for financial support of 500 MHz NMR spectrometer of Chimie-ParisTech in the framework of the SESAME equipment project (n°16016326).

## References

[1] M. M Lee, J. Teuscher, T. Miyasaka, T. N. Murakami, H. J. Snaith, *Science* **2012**, *338*, 643-647.

[2] H.-S. Kim, C.-R. Lee, J.-H. Im, L. K.-B. Lee, T. Moehl, A. Marchioro, S.-J. Moon, R. Humphry-Baker, J.-H. Yum, J. E. Moser, M. Grätzel, N.-G. Park, *Sci. Rep.* **2012**, *2*, 591.

[3] J. Burschka, N. Pellet, S.-J. Moon, R. Humphry-Baker, P. Gao, M. K. Nazeeruddin, M. Grätzel, *Nature* **2013**, *499*, 316.

[4] H. Zhou, Q. Chen, G. Li, S. Luo, T. Song, H.-S. Duan, Z. Hong, J. You, Y. Liu, Y. Yang, *Science* **2014**, *345*, 542-546.

[5] J. Zhang, P. Barboux, T. Pauporté, *Adv. Energy Mater.* **2014**, *4*, 1400932.

[6] J. Zhang, E. J. Juárez-Pérez, I. Mora-Seró, B. Viana, Th. Pauporté, *J. Mater. Chem. A* **2015**, *3*, 4909–4915.

[7] P. Wang, Z. Shao, M. Ulfa, T. Pauporté, *J. Phys. Chem. C* **2017**, *121*, 9131–9141.

[8] T. Zhu, J. Su, F. Labat, I. Ciofini, Th. Pauporté *ACS Appl. Mater Interfaces* **2020**, *12*, 744-752.

[9] F. Zhang, K. Zhu, *Adv. Energy Mater.* **2020**, 10, 1902579.

[10] A. Leblanc, N. Mercier, M. Allain, J. Dittmer, T. Pauporté, V. Fernandez, F . Boucher, M. Kepenekian, C. Katan, *ACS Appl. Mater. Interfaces*, **2019**, *11*, 20743-20751.

[11] D. Pitarch-Tena, T.T. Ngo, M. Vallés-Pelarda, T. Pauporté, I. Mora-Seró. *ACS Energy Lett*. **2018**, *3*, 1044−1048.

[12] NREL Chart (May 2022) https://www.nrel.gov/pv/cell-efficiency.html

[13] M. Kim, G.-H. Kim, T. K. Lee, I. W. Choi, H. W. Choi, Y. Jo, Y. J. Yoon, J.W. Kim, J. Lee, D. Huh, H. Lee, S. K. Kwak, J. Y. Kim, and D. S. Kim, *Joule* **2019**, *3*, 2179-2192.

[14] T. Zhu, D. Zheng, M.-N. Rager, T. Pauporté, *Sol. RRL* **2020**, *4*, 2000348.

[15] T. Zhu, D. Zheng, J. Liu, L. Coolen, Th. Pauporté, *ACS Appl. Mater. Interfaces* **2020**, *12*, 37197−37207

[16] J. Jeong, M. Kim, J. Seo, H. Lu, P. Ahlawat, A. Mishra, Y. Yang, M.A. Hope, F.T. Eickemeyer, M. Kim, Y.J. Yoon, I.W. Choi, B.P. Darwich, S.J. Choi, Y. Jo, J. H. Lee, B. Walker, S.M. Zakeeruddin, L. Emsley, U. Rothlisberger, A. Hagfeldt, D.S. Kim, M. Grätzel, J.Y. Kim, *Nature* **2021**, *592*, 381-385.

[17] M. Kim, J. Jeong, H. Lu, T.K. Lee, F. T. Eickemeyer, Y. Liu, I.W. Choi, S.J. Choi, Y. Jo, H.-B. Kim, S.-I Mo, Y.-K. Kim, H. Lee, N.G. An, S. Cho, W.R. Tress, S. M. Zakeeruddin, A. Hagfeldt, J.Y. Kim, M. Grätzel, D. S. Kim, *Science* **2022**, *375*, 302–306.

[18] W. Hui, L. Chao, H. Lu, F. Xia, Q. Wei, Z. Su, T. Niu, L. Tao, B. Du, D. Li, Y. Wang, H. Dong, S. Zuo , B. Li, W. Shi, X. Ran, P. Li, H. Zhang, Z. Wu, C. Ran, L. Song, G. Xing, X. Gao, J. Zhang, Y. Xia, Y. Chen, W. Huang, *Science* **2021**, *371*, 1359–1364.

[19] C. Luo, G. Zheng, F. Gao, X. Wang, Y. Zhao, X. Gao, and Q. Zhao, *Joule* **2022**, *6*, 240-257.

[20] Y. Li, Z. Chen, B. Yu, S. Tan, Y. Cui, H. Wu, Y. Luo, J. Shi, D. Li, Q. Meng. *Joule* **2022**, *6*, 676-689.

[21] S. Tan, T. Huang, I. Yavuz, R. Wang, T. W. Yoon, M. Xu, Q. Xing, K. Park, D.-K. Lee, C.-H. Chen, R. Zheng, T. Yoon, Y. Zhao, H.-C. Wang, D. Meng, J. Xue, Y. J. Song, X. Pan, N.-G. Park, J-W. Lee, Y. Yang, *Nature* **2022,** *605*, 268–273

[22] R. Azmi, E. Ugur, A. Seitkhan, F. Aljamaan, A.S. Subbiah, J. Liu, G.T. Harrison, M.I. Nugraha, M.K. Eswaran, M. Babics, Y. Chen, F. Xu, T.G. Allen, A. Rehman, C.-L. Wang, T.D. Anthopoulos, U. Schwingenschlögl, M. De Bastiani1, E. Aydin, S. De Wolf, Science, **2022,** 10.1126/science.abm5784 (2022).

[23] X. Li, W. Zhang, X. Guo, C. Lu, J. Wei, J. Fang, *Science* **2022**, *375*, 434–437.

[24] S.-H. Turren-Cruz, A. Hagfeldt, M. Saliba, *Science* **2018**, *362*, 449–453.

**Please cite this paper as** : D. Zheng, F. Chen, M.N. Rager, L. Gollino, B. Zhang, Th. Pauporté, What are Methylammonium and Solvent Fates upon Halide Perovskite Thin Film Preparation and Thermal Aging? Adv. Mater. Interfaces, (2022) 2201436. DOI : 10.1002/admi.202201436
[25] X. Wang, Y. Fan, L. Wang, C. Chen, Z. Li, R. Liu, H. Meng, Z. Shao, X. Du, H. Zhang, G. Cui, S. Pang, *Chem*. **2020**, *6*, 1369–1378.

[26] E.J. Juarez-Perez, L.K. Ono, I. Uriarte, E.J. Cocinero, Y. Qi, *ACS Appl. Mater. Interfaces* **2019**, *11*, 12586−12593.

[27] E.J. Juarez-Perez, Z. Hawash, S.R. Raga, L.K. Ono, Y. Qi, *Energy Environ. Sci*. **2016**, *9*, 3406−3410.

[28] L. Gollino, Th. Pauporté, *Sol. RRL* **2021**, *5*, 2000616.

[29] W. Travis, E.N.K. Glover, H. Bronstein, D.O. Scanlon, R.G. Palgrave, *Chem. Sci*. **2016**, *7*, 4548-4556.

[30] A. Leblanc, N. Mercier, M. Allain, J. Dittmer, V. Fernandez, T. Pauporté, Angew. Chem. Int. Ed., 2017, 56, 16067 –16072.

[31] L. Lei, M. Li, D. M. Grant, S. Yang, Y. Yu, J. A. Watts, D. B. Amabilino, *Chem. Mater*. **2020**, *32*, 5958−5972

[32] D. Zheng, T. Zhu, Y. Yan, Th. Pauporté**,** *Adv. Energy Mater*. **2022**, *12*, 2103618.

[33] J.S. Yun, J. Kim, T. Young, R. J. Patterson, D. Kim, J. Seidel, S Lim, M. A. Green, S.Huang, A. H. Baillie, *Adv. Funct. Mater* **2018**, *28*, 1705363

[34] Y. H. Park, I. Jeong, S. Bae, H. J. Son, P. Lee, J. Lee, C.-H. Lee, M.J. Ko, *Adv. Funct. Mater*. **2017**, *27*, 1605988

[35] D. Zheng, T. Pauporté, *J. Mater. Chem. A* **2021**, 9, 17801–17811.

[36] P. Wang, Z. Shao, M. Ulfa, T. Pauporté, *J. Phys. Chem. C*, **2017**, *121*, 9131–9141.

[37] Pauporté T., Finne J., Kahn-Harari A., Lincot D. *Surf. Coat. Technol*., **2005**, *199*, 213-219.

**Please cite this paper as** : D. Zheng, F. Chen, M.N. Rager, L. Gollino, B. Zhang, Th. Pauporté, What are Methylammonium and Solvent Fates upon Halide Perovskite Thin Film Preparation and Thermal Aging? Adv. Mater. Interfaces, (2022) 2201436. DOI : 10.1002/admi.202201436

## Table of Content

Methylammonium chloride additive in excess is ubiquitously employed for the preparation of very high efficiency perovskite solar cells. We unveil the reactivity of this additive with other A-site cations and its elimination process upon the perovskite film formation by thermal annealing. Thermal aging stress provokes further changes in the cation composition of the layer.